OPTOELECTRONICS AND ADVANCED MATERIALS – RAPID COMMUNICATIONS Vol. 1, No. 5, May 2007, p. 235 - 241

Fractal analysis of metal surfaces mechanically polished by several methods

T. SAKAI
Department of Mechanical Engineering, Takamatsu National College of Technology, 355 Chokushi, Takamatsu, Kagawa 761-8058 Japan

The roughness of a mechanically polished surface of any machine component is expected to depend both on finishing methods and evaluation procedures. Presumably, a surface finished using buff-polishing is flat and smooth compared to a surface finished using a shaper. Even if a surface is finished using a definite procedure, the roughness also depends on the measurement procedure. A surface looks flat and smooth after finishing by a given method if one observes by the naked eye. But the surface appears rough if one observes it using a high-resolution microscope. The roughness becomes more distinct with increased resolution of the microscope. This aspect can be attributed to a fractal nature of the mechanically finished metal surface. From this point of view, fractal analysis is applied to evaluate the geometric irregularity of polished surfaces using different methods of shaper finishing, milling, grinding, and buff-polishing. The results show that the geometric irregularity of the surface is well evaluated by combining the fractal dimension and additional indices that are peculiar to machining methods.

(Received March 20, 2007; accepted April 5, 2007)

Keywords: Fractal, Fractal dimension, Richardson effect, Metal surface, Surface finishing, Roughness, Scanning laser microscope

1. Introduction

To analyze the complexity quantitatively, various methods have been developed, and a selected method is typically applied for a certain phenomenon. Especially extreme irregular and complex shapes exist in nature. Such irregular phenomena have been evaluated using Fourier analysis or the theory of stochastic processes. On the other hand, to evaluate such irregular phenomena quantitatively, Mandelbrot proposed the new concept of "fractal" analysis [1, 2]; it has since been applied to various fields. This concept was initially thought to be applicable only for mathematical studies [3] and artistic applications [4] because of progress of computer graphics. Notwithstanding, this concept has recently been applied to various fields such as biology [2, 5], medical science [6], physical sciences [7], engineering [8–15], economics [16], and so on. Now the fractal dimension is defined as a quantitative measurement of irregularity. In general, the fractal dimension is defined as a parameter extended from an integral dimension characterized by Euclidean geometry. The common basic scope in these investigations, as mentioned above, is to quantify irregularity using the fractal dimension.

In this study, we applied this concept of fractals to evaluate geometric characteristics of mechanically polished surfaces. Especially, in this paper, this analysis is applied to evaluate the geometric irregularity of surfaces that have been finished using different methods of shapeing, finishing, milling, grinding, and buff-polishing. Consequently, the effectiveness of this analytical method proposed in this paper for the polished surfaces is confirmed.

2. Fractal analysis for shape irregularity of solid

The fundamental theory of fractals is now developing and is not thoroughly established. At its present stage, the fractal dimension is not unified to give a unique result. For that reason, many different definitions are accepted depending on the subject [17]. In this study, the following procedure was applied to analyze the fractal dimension. First, we considered that the Mesh method, concerning a closed irregular line in the plane, is extended to a new method to consider a solid problem. For closed complex lines in the plane such as trees, snowflakes, and coastlines that include complicated concave-convex shapes, if the *Richardson effect* [18], as verified by L. F. Richardson, is extended to an unknown field that represents a solid problem, then a line of reasoning will be established as follows. In the objective solid in the present stage, this solid is first divided into many small solids. If we decide that a side length of unit area element defined by the procedure described above is ε and that a number of solid passing solid surfaces is n, then the relationship between ε and n can be represented using the following equation if this solid under consideration has a fractal nature [2].

$$n=F\,\varepsilon^{-D} \tag{1}$$

Table 1. Numerical list of machining conditions.

(a) Shaper and milling

Finishing method	Feed speed (mm/min)
Shaper	1.6
	1.2
	0.8
	0.4
	0.2
Milling	60.0
	45.0
	40.0
	35.0
	24.0

(b) Grinding and buff-polishing

Finishing method	Cutting depth (μm)	Particle size (μm)
Grinding	20.0	250.0 (#60) (constant)
	15.0	
	10.0	
	5.0	
	3.0 (constant)	250.0
		96.0
		16.0
		7.9
Buff-polishing		1.00
		0.50
		0.30
		0.06

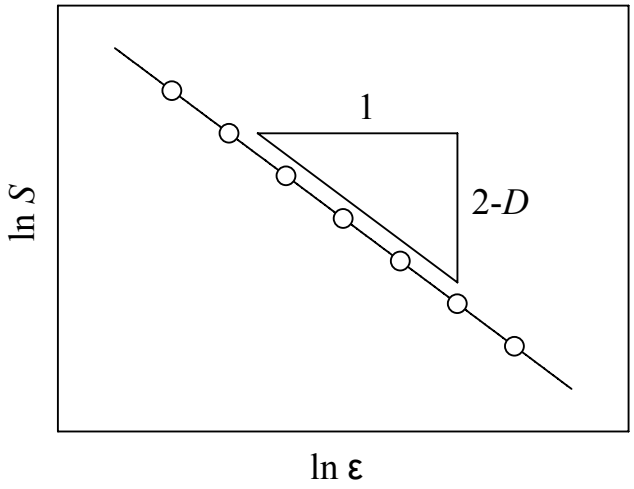

Fig. 1. Schematics of Richardson effect.

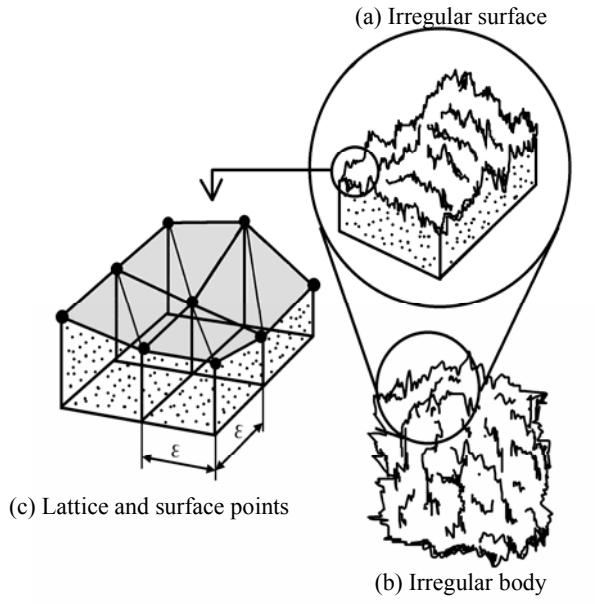

Fig. 2. Replacement of irregular surface by multifacet surface.

In that equation (1), F is a constant, and D is the fractal dimension. Therefore, because this surface area, which has a side length of ε, is given as ε^2 , surface area S, composed by complicated concave-convex surfaces, is represented as the following equation:

$$S=n\varepsilon^2=F\varepsilon^{2-D} \tag{2}$$

Thus, the whole surface area of a closed surface is approximated by polygonal surfaces. If we take logarithms for both sides of Eq. (2), we have replacement of the irregular surface by a multifaceted surface.

$$\ln S=\ln F+(2-D)\ln \varepsilon \tag{3}$$

If this irregular surface has a fractal nature, then the relationship between a side length of unit area element ε and a number of solid passing solid surfaces n must be represented as a straight line on ln ε-ln S coordinates, as shown schematically in Fig. 1. Therefore, fractal dimension D is depicted as the slope of the regression line in Fig. 1. This dimension D is always D larger than 2 because the regression line must have a negative slope. One implication is that a perfectly flat surface must have three dimensions: no matter how smooth a surface is, this solid having the irregular surface must have a real number dimension over three dimensions considered from the fractal point of view. The surface area S changes depending on the side length of unit area element ε; the effect of ε on the surface area S is the Richardson effect. In this study, the slope of the regression line corresponds to 2-D because the analytical object is a curved surface instead of the irregular curve in a plane. These concepts are applied to analysis of irregularities of a closed surface.

In this study, we applied this concept of fractals to evaluate the geometrical characteristics of a mechanically polished surface. This object corresponds to a plate having an irregular surface if we cut out a certain portion of the body, as shown in Fig. 2 (a). If we apply this concept of fractals continuously to an extensive region, mechanically polished surface irregularities can also be analyzed using an identical procedure, as described previously. Therefore, in this study, we performed a computer analysis for mechanically polished surface irregularities as follows.

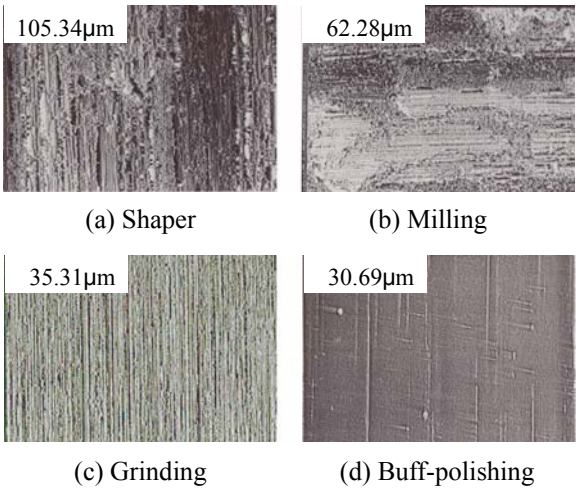

Fig. 3. Laser micrographs of the polished surfaces.

The surface of an irregular body in Fig. 2 (b) is replaced by a multifaceted surface consisting of numerous irregular facets. This object corresponds to a plate having the irregular surface if we cut out a certain portion of the body, as shown in Fig. 2 (a). Fig. 2 (c) shows that the irregular surface is finally provided by three-dimensional numerical data. Analytical results corresponding to the Richardson effect, as shown in Fig. 1, are provided if these numerical data are plotted on ln ε-ln *S* coordinates.

3. Specimens

The material used in this study is S45C carbon steel. Many specimens are prepared and finished using different methods of shaper finishing, milling, grinding, and buff-polishing. A list of machining conditions is shown in Table 1. In shaper finishing, the horizontal feeding rate is considered to be a controlling parameter. During milling, the feeding rate along the cutting direction is a controlling parameter under a constant revolution of 325 rpm with an 18.9φ endmill. For grinding, the cutting depth in each pass is a principal parameter. Here, we used a #60 grinding wheel. The average grain size is about 250 μm. The effect of the grain size of grinding wheel on roughness of the polished surfaces is also analyzed under a constant cutting depth of 3 μm. Finally, in buff-polishing, the alumina particle size is a controlling parameter because alumina particles are used to polish the surface after grinding.

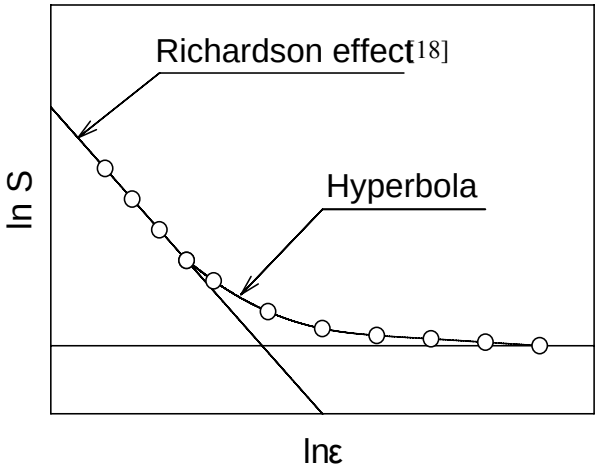

Fig. 4. Illustration of hyperbola model.

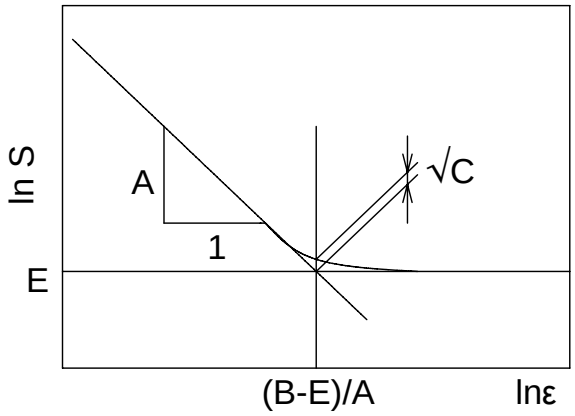

Fig. 5. Schematics of ln ε-ln S relationship [19].

Fig. 3 shows that these specimen surfaces, which are mechanically finished using respective methods, are observed using a laser microscope with 600× magnification. In these photographs, bright areas indicate high positions in the actual surface; dark areas indicate low positions. In real scale, the respective vertical and horizontal measurements in each photograph are 347.7 μm and 468.0 μm. Numerical values shown in the top-left area of each photograph indicate a difference between a low position and a high position using the micrometer scale. These photographs are composed of 110 × 148 dots divided into 256 phase shades. Therefore, these photographs are based on three-dimensional data of 4,167,680 points (110 dots × 148 dots × 256 phases).

A square area of 347.7 μm × 347.7 μm is defined as a sample area to analyze surface irregularity. This area is replaced by a 110dot×110dot CRT screen. Therefore, one dot on a laser microscope corresponds directly to one dot on a CRT screen: 1dot × 1dot on the CRT screen corresponds to a physical area of 3.16 μm × 3.16 μm on the surface.

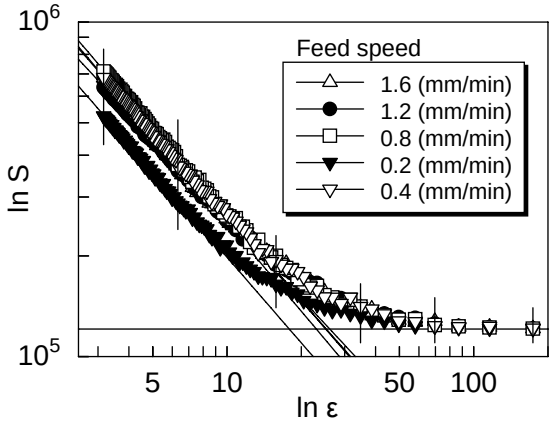

Fig. 6. ln ε-ln S relationships for shaper finishing.

Table 2. Analytical results for shaper finishing.

Feed speed (mm/min)	Fractal dimension *D*		Index of surface nature	
		A	B-E	C
1.6	2.88	0.88	20.1	1.45×10^{10}
1.2	2.79	0.79	20.6	7.65×10^{9}
0.8	2.86	0.86	21.6	9.58×10^{9}
0.4	2.85	0.85	15.2	1.15×10^{10}
0.2	2.84	0.84	21.1	8.44×10^{9}

In this analysis, the surface area is digitized into three-dimensional numerical data using a laser microscope. Based on the thus-digitized surface, the Richardson effect is analyzed and the fractal dimension is determined.

4. Analytical results and discussion

4.1 Fractal dimension and index of surface nature

Usually, the linear Richardson effect is confirmed within a limited range of ε. But the Richardson effect in the entire region of ε should be represented as a different type of equation. Therefore, we propose the following expression in hyperbola type [19].

$$(\ln S\text{-}E)(\ln S + A \ln \varepsilon\text{-}B)=C \quad (4)$$

Here the hyperbola type proposed in this study is shown in Fig. 4. These parameters, i.e., *B*, *C*, and *E* in Eq. (4), are precisely defined in Fig. 5 and illustrated diagrammatically. The fractal dimension is calculated from the regression line slope: A=2-D, for data points within the linear portion. The fractal dimension and parameters such as *B*, *C*, and *E* in Eq. (4) are analyzed using a curve-fitting technique. In this study, these parameters are designated as "indices of surface nature" because these parameters well reflect the geometrical characteristics of the mechanically polished surface. For the index of surface nature, *E*, this value provides the area of a perfect flat surface. Deterioration of another index, *C*, indicates the expansion of the region in which the linear Richardson effect is realized. Furthermore, the index, (*B*-*E*)/*A*, indicates the value of ln ε at the intersection.

4.2 Analytical results of surface irregularity for respective Finishing Methods

(1) Shaper finishing

For surface irregularities arising from shaper finishing, the relationship between ln ε and ln *S* obtained using the analytical procedures described above is shown in Fig. 6. For division of analytical area of 110dot × 110dot, if we assume the divided side length of unit area element ε=1dot, 2dot, 5dot, 11dot, 22dot, 55dot and so on, a side length of the analytical area is divided equally into 110partitions, 55partitions, 22partitions, and so on, respectively. Here, each plot on the vertical line in Fig. 6 provides the analytical result for divided ε (ε=3.16 μm, 6.32 μm, 15.80 μm, and so on).

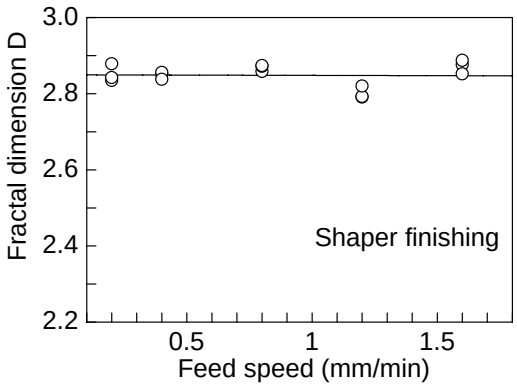

Fig. 7. Fractal dimension vs. feed speed.

This figure shows analytical results of surface irregularities for finishing conditions, that is the feeding rate, decreases linearly from a maximum surface area (analytical result located on top-left portion in this figure) with increasing divided ε. And this analytical result approaches index of surface nature *E*. The feeding rate in the case of shaper does not demonstrably influence the surface area of the polished surface because the order of the feeding rate does not necessarily correspond to the order of the plot for a maximum surface area in this figure. Solid lines, showing an index of surface nature *E* and a slanting asymptote, in this figure are equivalent to asymptotes in Eq. (4). A slanting asymptote is decided from the following procedure. For analytical results of the slanting region in this figure, the top-half region for analytical results where the linear Richardson effect is realized by the naked eye is approximated using least-squares method. Therefore, we that this approximated line corresponds to a slanting asymptote. Fractal dimension *D* is provided by the slope of a slanting asymptote, as described previously. The index of surface nature *A* well corresponds to fractal dimension *D*: A=2-D. Regarding the index of surface nature *E*, this value provides the area of perfect flat surface, as mentioned previously; in this case, this value provides a constant value, E=ln (1.21×10^5) because the analytical area is intended for a square area of 347.7 μm × 347.7 μm as a sample area.

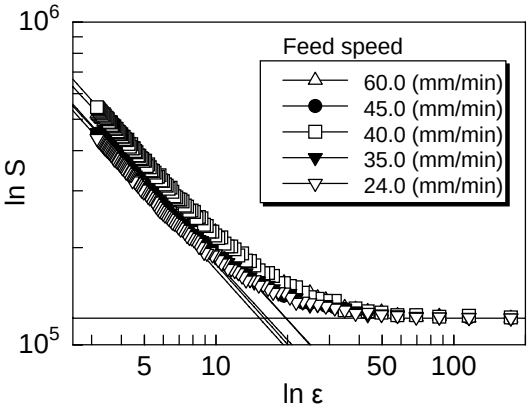

Fig. 8. ln ε-ln S relationships for milling.

Table 3. Analytical results for milling.

Feed speed (mm/min)	Fractal dimension *D*	Index of surface nature		
		A	B-E	C
60.0	2.80	0.80	15.8	1.17×10^{10}
45.0	2.80	0.80	13.2	1.02×10^{10}
40.0	2.83	0.83	16.3	1.12×10^{10}
35.0	2.82	0.82	13.1	1.09×10^{10}
24.0	2.82	0.82	12.5	9.88×10^{9}

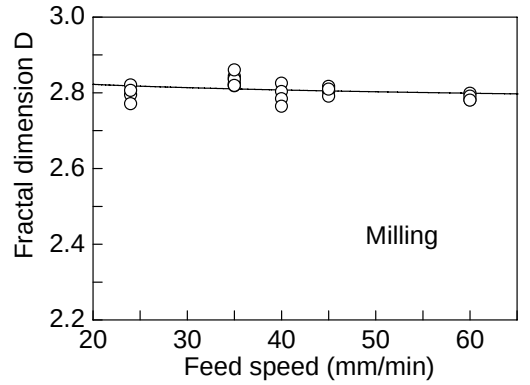

Fig. 9. Fractal dimension vs. feed speed.

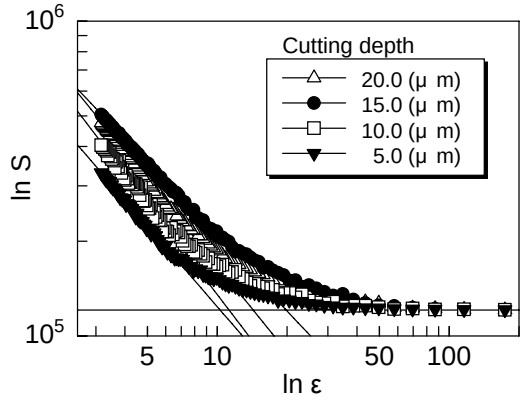

Fig. 10. ln ε-ln S relationships for grinding.

Table 4. Analytical results for grinding.

Cutting depth (μm)	Fractal dimension *D*		Index of surface nature	
		A	B-E	C
20.0	2.91	0.91	13.0	1.44×10^{10}
15.0	2.78	0.78	15.4	1.18×10^{10}
10.0	2.97	0.97	10.9	1.34×10^{10}
5.0	2.85	0.85	8.76	8.62×10^{9}

Table 2 is a list of analytical results for shaper finishing such as the fractal dimension and each index of the surface nature. Fig. 7 shows the relationship between the fractal dimension and the feeding rate to recognize the influence of each finishing condition. In this figure, for surface irregularities arising from finishing using a shaper, the fractal dimension and each index of surface nature are almost constant, irrespective of the feeding rate. Therefore, the surface irregularity of a material, when finished using a shaper, is not dependent on the feeding rate.

(2) Milling

Fig. 8 shows the relationship between ln ε and ln *S*, as analyzed using the procedure as described above for surface irregularity when the material is finished by milling. In Fig. 8, this figure is also corrected using the procedure described above, but the expression of the vertical line is not represented to avoid complications (as above). In this figure, for surface irregularities finished by milling at each feeding rate, the relationship between ln ε and ln *S* is well represented using a hyperbola, as in Fig. 6.

Table 3 shows a list of analytical results for milling, such as the fractal dimension and each index of surface nature. Fig. 9 shows the relationship between the fractal dimension and the feeding rate for milling. In this figure, for surface irregularity from a material finished by milling, the fractal dimension and each index of surface nature are almost constant, irrespective of the feeding rate, as with shaper finishing. Therefore, the surface irregularity from a material finished by milling is also not dependent on the feeding rate in this investigation, as with shaper finishing. In Fig. 6 and Fig. 8, these facts demonstrate that analytical results for each feeding rate are well represented as a hyperbola.

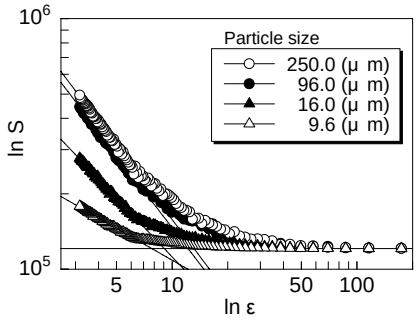

Fig. 11. ln ε-ln S relationships for grinding.

Table 5. Analytical results for grinding.

Particle size (μm)	Fractal dimension *D*	Index of surface nature		
		A	B-E	C
250.0	2.92	0.92	12.0	1.45×10^{10}
96.0	2.90	0.90	11.0	1.21×10^{10}
16.0	2.70	0.70	6.33	4.70×10^{9}
7.9	2.36	0.36	2.82	8.41×10^{9}

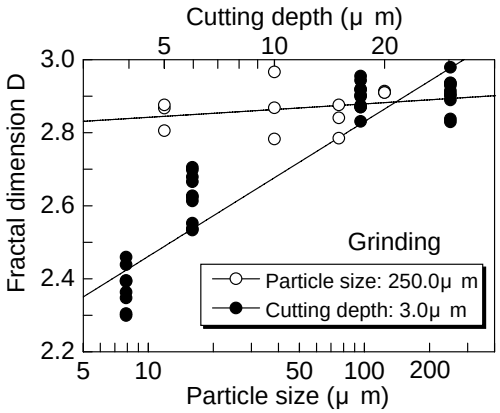

Fig. 12. Variation of fractal dimension due to cutting depth and particle size.

(3) Grinding

Fig. 10 shows analytical results of surface irregularity for a material finished by grinding with a #60 grinding wheel. In this case, the grain size is constant, but the cutting depth is varied to reflect the influence of the cutting depth. Table 4 presents a list of analytical results for grinding such as the fractal dimension and each index of the surface nature. Fig. 10 shows a similar pattern to those of the two finishing methods described above: the relationship between ln ε and ln *S* for grinding is well represented as a hyperbola, but the slope of a slanting asymptote is very dispersed. The order of plots of a maximum surface area does not correspond to the order of the cutting depth of the grinding wheel.

Here, for interest, in the case of grinding, analytical results finished by grinding under a constant cutting depth of 3 μm are shown in Fig. 11. Table 5 presents a list of analytical results for grinding under a constant cutting depth of 3 μm. Plots of ● in Fig. 12 show the relationship between the fractal dimension and the grinding-wheel grain size. As shown in this figure, the fractal dimension increases with increased cutting depth of grinding wheel. Furthermore, plots of ○ in this figure provide analytical results for varying the cutting depth under a constant 250.0 μm grain size of the grinding wheel, based on results of Table 4. For plots of ○ in this figure, the fractal dimension is almost constant irrespective of cutting depth. These facts indicate the same trend toward analytical results as those for shaper finishing and milling, meaning that the fractal dimension increases with increased grain size of the grinding wheel: the polished surface area also increases with increased grain size of the grinding wheel.

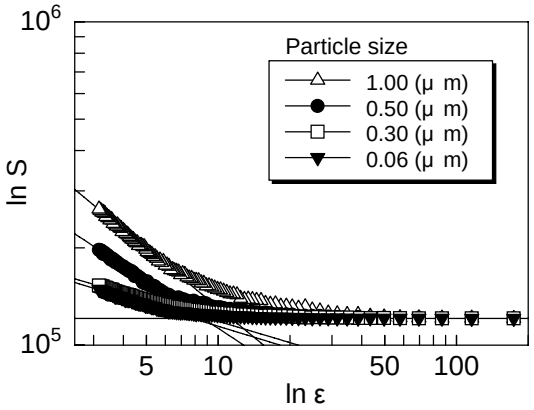

Fig. 13. ln ε-ln S relationships for buff-polishing.

Table 6. Analytical results for buff-polishing

Particle size (μm)	Fractal dimension *D*		Index of surface nature	
		A	B-E	C
1.00	2.61	0.61	6.89	5.18×10^{9}
0.50	2.49	0.49	4.20	1.93×10^{9}
0.30	2.22	0.22	1.99	2.69×10^{8}
0.06	2.23	0.23	1.75	2.35×10^{8}

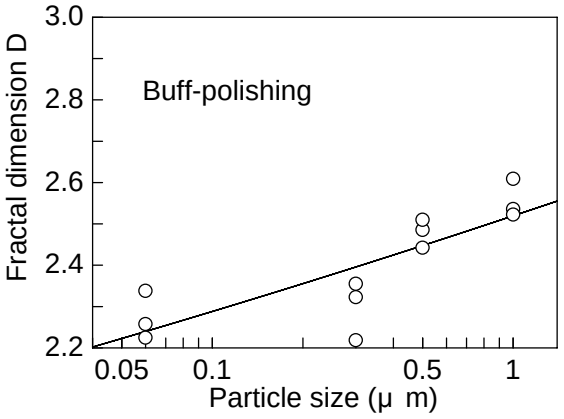

Fig. 14. Fractal dimension vs. particle size.

(4) Buff-polishing

Fig. 13 shows analytical results for surfaces finished using buff-polishing with four kinds of aluminum particles: 1.00 μm, 0.50 μm, 0.30 μm, and 0.06 μm. Table 6 lists analytical results for buff-polishing such as the fractal dimension along with each index of surface nature. Fig. 14 shows the relationship between the obtained fractal dimension and the alumina particle grain

size. In this figure, the fractal dimension D increases with increased particle size. Here, in Fig. 7, Fig. 9, Fig. 12, and Fig. 14, to compare the fractal dimension directly, we unified a scale of the vertical axis for each figure of ln ε-ln S relationships.

Fig. 13 shows that the slope of a slanting asymptote varies with alumina particle size. This tendency is identical to that for analytical results for grinding with varying size of the grinding wheel. This figure shows that the surface area of the polished surface is heavily dependent on the alumina particle size because the order of plots for a maximum surface area well corresponds to the order of alumina particle size. In addition, in Table 6, for surface irregularity finished by buff-polishing, the fractal dimension and each index of surface nature decreases with decreasing alumina particle size. The values in buff-polishing are much smaller than those in the cases using shaping, milling, and grinding.

Regarding the relationship between ln ε and ln S for polished surface irregularity, analytical results in each finishing method show the Richardson effect precisely. With increasing side length of square area as a sample area, the surface area of analytical results decreases linearly in the log-normal scale at first. Therefore, a fractal nature for polished surface irregularity is confirmed. Because the side length of the square area is sufficiently extended, the surface area approximates step by step to a perfect flat surface that has an index of surface nature E. The relationship between ln ε and ln S for a polished surface is well approximated as a hyperbola. Results show that the geometrical irregularity of the surface is well evaluated by combining the fractal dimension and additional indices that are peculiar to each finishing method.

5. Conclusions

An analytical procedure to evaluate the surface irregularity of a polished surface was developed by applying a fractal concept and a curve-fitting technique. Main conclusions obtained in this study are summarized as follows:

We confirmed that the metal surfaces finished by different methods of shaper finishing, milling, grinding, and buff-polishing have a fractal nature.

Results show that the geometrical irregularity of the surfaces is well evaluated by combining the fractal dimension and additional indices that are peculiar to the finishing methods.

For shaping, milling, and grinding, the fractal dimension is almost constant, irrespective of the finishing conditions. But for buff-polishing and the case of grinding, the fractal dimension increases with increased particle size.

References

[1] B. B. Mandelbrot, Fractals: Form, Chance and Dimension, W. H. Freeman and Company, San Francisco, (1977), pp. 1-27.
[2] B. B. Mandelbrot, The Fractal geometry of Nature, W. H. Freeman and Company, New York, (1983), pp. 1-20.
[3] H. Takayasu, Fractal, Asakura-shoten, Japan, (1986), pp. 1-31.
[4] H. O. Peitgen and P. H. Richter, The Beauty of Fractals, Springer-Verlag, Berlin, (1986), pp. 23-125.
[5] H. Takayasu, I. Nishikawa, Proceedings of 1st International Symposium, Science on Form, (1986), pp. 15-16.
[6] B. J. West, A. L. Goldberger, American Scientist **75**, 354 (1987).
[7] B. B. Mandelbrot, Journal of Statistical Physics **34**, 895 (1984).
[8] T. Sakai, M. Ramulu, A. Ghosh, R. C. Bradt., International Journal of Fracture **48**, 49 (1991).
[9] J. J. Mecholsky, D. E. Passoja, K. S. Feinberg-Ringel Journal of American Ceramics Society, **72**, 60 (1989).
[10] T. Sakai, M. Fujikawa, S. L. Mcintyre, R. C. Bradt Materials Science Research International, **2**(4), 235 (1996).
[11] T. Sakai, M. Fujikawa, Journal of the Society of Materials Science Japan, **41**, 1605 (1992).
[12] S. Matsuoka, H. Sumiyoshi, K. Ishikawa, Transaction of Japan Society of Mechanical Engineering, **56**, 2091 (1990).
[13] S. Matsuoka, Journal of the Society of Materials Science Japan **42**, 1245 (1993).
[14] M. Tsuda, Y. Hirose, Z. Yajima, K. Tanaka, Journal of the Society of Materials Science Japan, **37**, 599 (1988).
[15] M. Tsuda, Y. Hirose, M. Kurose, S. Matsuoka, T. Kurobe, K. Tanaka, Journal of the Society of Materials Science Japan, **40**, 100 (1991).
[16] E. W. Montroll, M. F. Shelesinger, Journal of Statistical Physics **32**, 209 (1983).
[17] H. Takayasu, Fractal, Asakura-shoten, Japan, (1986), p. 154.
[18] L. F. Richardson, General System Yearbook, **6**, 139 (1961).
[19] S. Nishijima, Transaction of Japan Society of Mechanical Engineering **46**, 1303 (1990).

*Corresponding author: sakai@takamatsu-nct.ac.jp